Polymer Chemistry

PAPER

Cite this: *Polym. Chem.*, 2015, **6**, 4775

Pyridine-bridged diketopyrrolopyrrole conjugated polymers for field-effect transistors and polymer solar cells†

Xiaotao Zhang,[a] Chengyi Xiao,[a] Andong Zhang,[a] Fangxu Yang,[a] Huanli Dong,[a] Zhaohui Wang,[a] Xiaowei Zhan,[b] Weiwei Li*[a] and Wenping Hu*[a,c]

Received 12th April 2015,
Accepted 22nd May 2015

DOI: 10.1039/c5py00538h

www.rsc.org/polymers

Five wide or medium band gap diketopyrrolopyrrole (DPP)-based conjugated polymers with pyridine as bridges were developed for organic field-effect transistors (OFETs) and polymer solar cells (PSCs). By introducing copolymerized aromatic building blocks from strong electron-donating units to electron-deficient units into the conjugated backbone, the highest occupied molecular orbital (HOMO) and lowest unoccupied molecular orbital (LUMO) levels of the DPP polymers were tailored to the low-lying position. Therefore, the polarity of charge transport in OFETs can be switched from p-type to n-type. The DPP polymer with a low-lying LUMO of −3.80 eV provides a hole-only mobility of 2.95×10^{-2} cm^2 V^{-1} s^{-1}, while an electron-only mobility of 1.24×10^{-3} cm^2 V^{-1} s^{-1} is found in the DPP polymer with a LUMO of −4.22 eV. Further investigation of photovoltaic cells based on these DPP polymers shows a modest power conversion efficiency (PCE) of around 2%. Our results demonstrate that wide band gap pyridine-bridged DPP polymers have potential application in OFETs and OSCs by adjusting their energy level with alternated units on the conjugated backbone.

Introduction

Diketopyrrolopyrrole (DPP) based conjugated polymers have been intensively investigated for their application in organic electronics, such as organic field-effect transistors (OFETs)[1] and polymer solar cells (PSCs),[2] since 2008.[3] DPP derivatives were prepared from aromatic nitriles with succinic acid diesters,[4] where aromatic units as a bridge have a crucial influence on the properties of DPP polymers. Thienyl-bridged DPP polymers are mostly reported with high hole[5–8] and electron mobilities[9] above 1 cm^2 V^{-1} s^{-1} in OFETs and PCE up to 8% in PSCs.[10,11] Analogues of thiophene, such as thienothiophene,[11–13] selenophene,[14,15] furan[16–18] and thiazole,[19,20] were also applied as bridges for DPP polymers to show promising performance in OFETs and PSCs. Electron donating thiophene and its analogue as a bridge combined with a strong electron deficient DPP core easily provide DPP polymers near-infrared absorption up to 1000 nm,[14] which is especially beneficial for tandem and multi-junction solar cells.[21–24] In another aspect, DPP polymers show excellent crystallinity and high charge carrier mobilities that make them interesting to be explored as wide band gap polymers for OFETs and PSCs, but related polymers are rarely studied.[25–27]

Conjugated polymers alternating with an electron donor and an electron acceptor are widely reported toward tunable absorption spectra and the energy level *via* internal charge transfer.[28] A DPP core with a strong electron deficient ability requires weak donating units to form a wide band gap polymer. When thienyl-bridged DPP polymers are copolymerized with weak donors, such as biphenyl units,[26] carbazole[29,30] and fluorene[31–33] derivatives, the absorption onset of DPP polymers can be tuned to around 750 nm. Further blue-shifted absorption spectra to the visible region for DPP polymers desire the modification of bridges with a weak donating ability compared to thiophene. Phenyl-bridged DPP polymers as wide band gap materials are widely reported for the application of pigment,[34] photo- or electron-luminescence,[35,36] but show poor performance in OFETs[37] and PSCs (lower than 2%).[25,38,39] The dihedral angle between the phenyl unit and the DPP core of around 30° makes the twist conjugated backbone of DPP polymers that will influence the crystallinity and charge transport.[40]

[a]*Beijing National Laboratory for Molecular Sciences, CAS Key Laboratory of Organic Solids, Institute of Chemistry, Chinese Academy of Sciences, Beijing 100190, P. R. China. E-mail: liweiwei@iccas.ac.cn, huwp@iccas.ac.cn*

[b]*Department of Materials Science and Engineering, College of Engineering, Peking University, Beijing 100871, China*

[c]*Collaborative Innovation Center of Chemical Science and Engineering (Tianjin) & Department of Chemistry, School of Science, Tianjin University, Tianjin 300072, China*

†Electronic supplementary information (ESI) available. See DOI: 10.1039/c5py00538h

The dihedral angle of phenyl-bridged DPP units originated from the adjacent H atom on the phenyl unit and the methyl group attached to the amide of the DPP core, which can be eliminated *via* replacing benzene by pyridine.[27] Wide band gap DPP polymers can be made with pyridine as the bridge due to its similar donating ability to benzene. In addition, the electron-withdrawing amine group (C═N) at the pyridine unit also helps DPP polymers achieve deep highest occupied molecular orbital (HOMO) and lowest unoccupied molecular orbital (LUMO) levels that are especially beneficial for high open circuit voltage (V_{oc}) in PSCs. Pyridine-bridged DPP polymers have been reported for high electron mobilities of 6.3 $cm^2 V^{-1} s^{-1}$ for OFETs[41] and PSCs with a PCE of 4.9%.[27] It will be useful to further explore the pyridine-bridged DPP polymers for application in OFETs and PSCs.

In this work, we systematically design and synthesis a series of pyridine-bridged DPP polymers alternating with a variety of different aromatic units (Fig. 1). All the polymers have wide or medium band gaps (1.41–1.85 eV), and their HOMO and LUMO levels were increased by reducing the electron donating ability or increasing the electron withdrawing ability of alternating aromatic units. **PDPP2Py2oT** with the strongly donating dimethyoxy-bithiophene (2oT) has low LUMO and HOMO levels of −3.87 eV and −5.28 eV, show p-type OFETs. When using weak donors such as benzodithiophene (BDT) and thiophene (T), **PDPP2PyBDT** and **PDPP2PyT** show ambipolar OFETs. Further increasing HOMO and LUMO levels can be realized by introducing the electron withdrawing benzothiadiazole (BTD) and naphthadiimide (NDI) into DPP polymers. **PDPP2PyNDI** has the deepest LUMO and HOMO levels (−4.22 eV and −6.07 eV) with n-type OFETs. Pyridine-bridged DPP polymers were also applied in PSCs with PCE up to 2.4%. We demonstrate that by modifying the molecular polarity of copolymerized units on the conjugated backbone of DPP polymers, the energy level and polarity of charge transport can be varied and hence influence their properties in OFETs and PSCs.

Experimental

Materials and measurements

All synthetic procedures were performed under a nitrogen (N_2) atmosphere. Commercial chemicals were used as received. THF and toluene were distilled from sodium under an N_2 atmosphere and benzophenone was used as the indicator. [6,6]-Phenyl-C71-butyric acid methyl ester ([70]PCBM) was purchased from Solenne BV. The monomer 4,9-dibromo-2,7-dioctylbenzo[*lmn*][3,8]phenanthroline-1,3,6,8(2*H*,7*H*)-tetraone, (4,8-bis(5-(2-ethylhexyl)thiophen-2-yl)benzo[1,2-*b*:4,5-*b*′]dithiophene-2,6-diyl)bis(trimethylstannane) (**4**), 2,5-bis(trimethylstannyl)thiophene (**5**) and 4,7-bis(4,4,5,5-tetramethyl-1,3,2-dioxaborolan-2-yl)benzo[*c*][1,2,5]thiadiazole (**6**) were purchased from Sunatech Inc. and recrystallized for polymerization. 3,6-Bis(5-bromopyridin-2-yl)-2,5-bis(2-octyldodecyl)pyrrolo[3,4-*c*]-pyrrole-1,4(2*H*,5*H*)-dione (**1**)[27] and (3,3′-dimethoxy-[2,2′-bithiophene]-5,5′-diyl)bis(trimethylstannane) (**2**)[42] were synthesized according to literature procedures.

^{1}H-NMR and ^{13}C-NMR spectra were recorded at 400 MHz and 100 MHz on a Bruker ANACE spectrometer with $CDCl_3$ as the solvent and tetramethylsilane (TMS) as the internal standard. The molecular weight of DPP polymers was determined with GPC at 140 °C on a PL-GPC 220 system using a PL-GEL 10 μm MIXED-B column and *ortho*-dichlorobenzene (*o*-DCB) as the eluent against polystyrene standards. A low concentration of 0.1 mg mL^{-1} polymer in *o*-DCB was applied to reduce aggregation. Electronic spectra were recorded on a JASCO V-570 spectrometer. Cyclic voltammetry was performed under an inert atmosphere with a scan rate of 0.1 V s^{-1} and 1 M tetrabutylammonium hexafluorophosphate in *o*-DCB as the electrolyte. The working, counter and reference electrodes were glassy carbon, Pt wire and Ag/AgCl, respectively. The concentration of the sample in the electrolyte was approximately 1 mM, based on monomers. All potentials were corrected against Fc/Fc^+. X-Ray diffraction (XRD) measurements were carried out in reflection mode at 40 kV and 200 mA with Cu Kα radiation

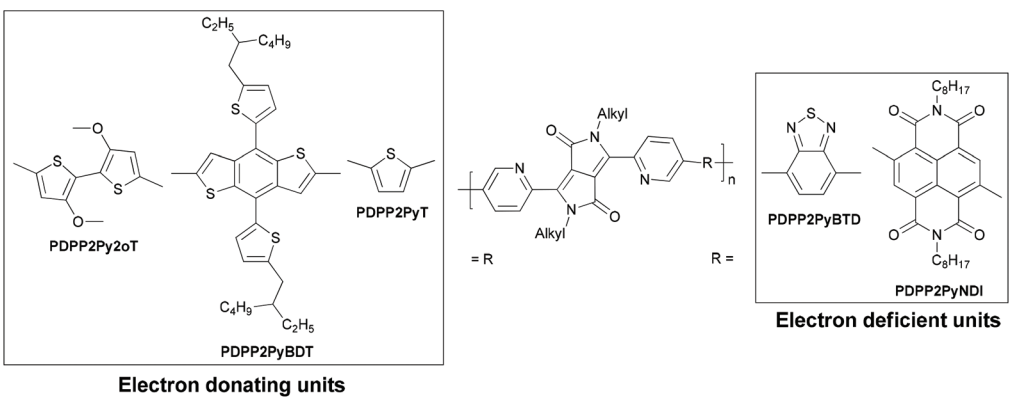

Fig. 1 Chemical structures of pyridine-bridged DPP polymers. Alkyl = octyldodecyl (OD) for **PDPP2Py2oT** and alkyl = hexyldecyl (HD) for other polymers.

using a 2 kW Rigaku D/max-2500 X-ray diffractometer. Grazing incidence wide-angle X-ray scattering (GIWAXS) experiments were conducted using XEUSS SAXS/WAXS equipment. Density function theory (DFT) calculations were performed at the B3LYP/6-31G* level of theory by using the Gaussian 09 program package. Atom force microscopy (AFM) images of films were obtained by using a Digital Instruments Nanoscope IIIa Multimode atomic force microscope in tapping mode.

Organic field-effect transistors were fabricated using heavily doped silicon wafers as the common gate electrode with a 300 nm thermally oxidized SiO_2 layer which was modified by OTS as the gate dielectric. Electrodes of Au (25 nm) were vacuum deposited first and then polymer thin films were spin coated on the substrate from *o*-DCB or chloroform solution with a thickness of around 30–50 nm, and then moved into a glovebox filled with N_2. After thermal annealing at the corresponding temperature, the devices were measured on an Agilent B1500 semiconductor parameter analyzer at room temperature.

Photovoltaic devices were made by spin coating poly(ethylenedioxythiophene):poly(styrene sulfonate) (PEDOT:PSS) (Clevios P, VP AI 4083) onto precleaned, patterned indium tin oxide (ITO) substrates (15 Ω per square). The photoactive layer was deposited by spin coating a chloroform solution containing the polymers and [70]PCBM with a 1 : 2 (w/w) ratio and appropriate amounts of 1,8-diiodooctane (DIO), 1-chloronaphthalene (1-CN) or *o*-DCB. Ca (20 nm) and Al (100 nm) were deposited by vacuum evaporation at $\sim 1 \times 10^{-5}$ Pa as the back electrode. The active area of the cells was 0.04 cm^2. An XES-70S1 (SAN-EI Electric Co., Ltd) solar simulator (AAA grade, 70 × 70 mm^2 photobeam size) coupled with AM 1.5 G solar spectrum filters was used as the light source, and the optical power at the sample was 100 mW cm^{-2}. A 2 × 2 cm^2 monocrystalline silicon reference cell (SRC-1000-TC-QZ) was purchased from VLSI Standards Inc. The current–voltage (*I–V*) measurement of the devices was conducted using a computer-controlled Agilent B2912A Precision Source/Measure Unit. The external quantum efficiency (EQE) spectrum was measured using a Solar Cell Spectral Response Measurement System QE-R3011 (Enlitech Co., Ltd). The light intensity at each wavelength was calibrated using a standard single crystal Si photovoltaic cell.

3,6-Bis(5-bromopyridin-2-yl)-2,5-bis(2-hexyldecyl)pyrrolo[3,4-*c*]pyrrole-1,4(2*H*,5*H*)-dione (3). To a degassed solution of 3,6-bis(5-bromopyridin-2-yl)pyrrolo[3,4-*c*]pyrrole-1,4(2*H*,5*H*)-dione[27] (1.99 g, 4.44 mmol) in *N*,*N*-dimethylformamide (50 mL), anhydrous potassium carbonate (1.85 g, 13.4 mmol) was added and heated under argon protection. 2-Hexyldecyl bromide (4.08 g, 13.4 mmol) was injected in one portion by a syringe. After the reaction was stirred for 12 h at 140 °C, the solution was cooled to room temperature, poured into 500 mL of ice water, and then extracted with CH_2Cl_2. After being dried in a vacuum, the crude product was purified by silica gel chromatography using dichloromethane as an eluent to obtain a red solid powder (1.4 g, 35%). ^{1}H NMR (400 MHz, $CDCl_3$) δ 8.92 (d, 2H), 8.74 (d, 2H), 8.01 (dd, 2H), 4.28 (d, 4H), 1.60 (s, 2H), 1.22 (d, 54H), 0.85 (dd, 12H). ^{13}C NMR (100 MHz, $CDCl_3$) δ 162.77, 150.40, 146.34, 145.27, 139.99, 128.74, 122.87, 111.71, 46.55, 38.50, 32.19, 32.10, 31.72, 30.29, 29.96, 29.84, 29.61, 26.61, 22.96, 14.40. MS (MALDI): calculated: 896.92, found: 896.9(M^+). Anal. Calcd for $C_{48}H_{72}Br_2N_4O_2$: C, 64.28; H, 8.09; N, 6.25. Found: C, 64.46; H, 8.07; N, 6.14.

2,7-Dioctyl-4,9-bis(tributylstannyl)benzo[*lmn*][3,8]phenanthroline-1,3,6,8(2*H*,7*H*)-tetraone (7). A solution of 4,9-dibromo-2,7-dioctylbenzo[*lmn*][3,8]phenanthroline-1,3,6,8-(2*H*,7*H*)-tetraone (0.500 g, 0.77 mmol), hexabutyldistannane (1.00 g, 1.73 mmol), and tri-*o*-tolylphosphine (0.051 g, 0.169 mmol) in toluene (10 mL) was deoxygenated with N_2. Tris(dibenzylideneacetone)dipalladium ($Pd_2(dba)_3$) (0.039 g, 0.042 mmol) was added and the reaction was heated to 90 °C overnight. Additional portions of tri-*o*-tolylphosphine (0.051 g, 0.169 mmol) and $Pd_2(dba)_3$ (0.039 g, 0.042 mmol) were added and the reaction was stirred at 90 °C for an additional 2 d. After cooling, the reaction mixture was filtered through a plug of silica gel eluting with dichloromethane/petroleum ether (1 : 2) and the solvent was removed under reduced pressure. The crude product was recrystallized from methanol to yield a light yellow solid (0.180 g, 22%). ^{1}H NMR (400 MHz, $CDCl_3$) δ 8.95 (s, 2H), 4.27–4.12 (m, 4H), 1.78–1.61 (m, 4H), 1.62–1.48 (m, 12H), 1.46–1.18 (m, 44H), 0.87 (t, J = 7.3 Hz, 24H). ^{13}C NMR (100 MHz, $CDCl_3$) δ 164.12 (s), 138.35 (s), 132.16 (s), 41.24 (s), 32.13 (s), 29.54 (t, J = 8.9 Hz), 28.43 (s), 27.71 (s), 27.35 (s), 22.93 (s), 14.37 (s), 14.01 (s), 11.86 (s). Anal. Calcd for $C_{54}H_{90}N_2O_4Sn_2$: C, 60.69; H, 8.49; N, 2.62. Found: C, 61.01; H, 8.46; N, 2.69.

PDPP2Py2oT. To a degassed solution of monomer **1** (211.87 mg, 0.21 mmol), (3,3′-dimethoxy-[2,2′-bithiophene]-5,5′-diyl)bis(trimethylstannane) (**2**) (115.87 mg, 0.21 mmol) in toluene (4 mL) and DMF (0.4 mL), $Pd_2(dba)_3$ (5.77 mg, 6.3 μmol) and triphenylphosphine (PPh_3) (6.61 mg, 25.2 μmol) were added. The mixture was stirred at 115 °C for 24 h, after which it was precipitated in methanol and filtered through a Soxhlet thimble. The polymer was extracted with acetone, hexane, dichloromethane and chloroform. The chloroform fraction was reduced and the polymer was precipitated in acetone. The polymer was collected by filtering over a 0.45 μm PTFE membrane filter and dried in a vacuum oven to yield **PDPP2Py2oT** (160 mg, 71%) as a dark solid. GPC (*o*-DCB, 140 °C): M_n = 9.9 kg mol^{-1}, PDI = 6.63. Anal. Calcd for $C_{66}H_{96}N_4O_4S_2$: C, 73.83; H, 9.01; N, 5.22. Found: C, 72.81; H, 8.86; N, 5.10.

PDPP2PyBDT. The same procedure as that for **PDPP2Py2oT** was used, but now **3** (159.31 mg, 0.18 mmol) and (4,8-bis(5-(2-ethylhexyl)thiophen-2-yl)benzo[1,2-*b*:4,5-*b*′]dithiophene-2,6-diyl)bis(trimethylstannane) (**4**) (160.74 mg, 0.18 mmol) were used as the monomers. Yield: 98.2 mg, 42%. GPC (*o*-DCB, 140 °C): M_n = 24.1 kg mol^{-1}, PDI = 3.13. Anal. Calcd for $C_{82}H_{112}N_4O_2S_4$: C, 74.95; H, 8.59; N, 4.26. Found: C, 74.40; H, 8.65; N, 4.19.

PDPP2PyT. The same procedure as that for **PDPP2Py2oT** was used, but now **3** (193.62 mg, 0.22 mmol) and 2,5-bis(trimethylstannyl)thiophene (**5**) (88.35 mg, 0.22 mmol) were used as the

monomers. Yield: 124.5 mg (70%). GPC (*o*-DCB, 140 °C): M_n = 24.5 kg mol^{-1}, PDI = 2.75. Anal. Calcd for $C_{52}H_{74}N_4O_2S$: C, 76.24; H, 9.10; N, 6.84. Found: C, 75.78; H, 8.95; N, 6.73.

PDPP2PyBTD. To a degassed solution of monomer **3** (143.88 mg, 0.016 mmol), 4,7-bis(4,4,5,5-tetramethyl-1,3,2-dioxaborolan-2-yl)benzo[*c*][1,2,5]thiadiazole (**6**) (62.29 mg, 0.16 mmol) in H_2O (0.5 mL) and toluene (5 mL) containing 2 M K_2CO_3, tetrakis(triphenylphosphine)palladium(0) ($Pd(PPh_3)_4$) (10.75 mg, 9.3 μmol) were added. The mixture was stirred at 80 °C for 24 h, after which it was precipitated in methanol, washed with water, and filtered through a Soxhlet thimble. The polymer was extracted with acetone, hexane, and chloroform. The chloroform fraction was reduced and the polymer was precipitated in acetone. The polymer was collected by filtering over a 0.45 μm PTFE membrane filter and dried in a vacuum oven to yield **PDPP2PyBTD** (57 mg, 41%) as a dark solid. GPC (*o*-DCB, 140 °C): M_n = 6.1 kg mol^{-1}, PDI = 2.49. Anal. Calcd for $C_{54}H_{74}N_6O_2S$: C, 74.44; H, 8.56; N, 9.65. Found: C, 71.60; H, 8.48; N, 8.99.

PDPP2PyNDI. To a degassed solution of monomer **3** (100 mg, 0.11 mmol), 7 (119 mg, 0.11 mmol) in toluene (3 mL) and DMF (0.3 mL), $Pd_2(dba)_3$ (3.02 mg, 3.3 μmol), PPh_3 (3.46 mg, 13.2 μmol) and CuI (4.19 mg, 22 μmol) were added. The mixture was stirred at 115 °C for 24 h, after which it was precipitated in methanol and filtered through a Soxhlet thimble. The polymer was extracted with acetone and hexane. The polymer was dissolved in chloroform and then precipitated in acetone. The polymer was collected by filtering over a 0.45 μm PTFE membrane filter and dried in a vacuum oven to yield **PDPP2PyNDI** (93 mg, 68%) as a dark solid. GPC (*o*-DCB, 140 °C): M_n = 15.2 kg mol^{-1}, PDI = 2.39. Anal. Calcd for $C_{78}H_{108}N_6O_6$: C, 76.43; H, 8.88; N, 6.86. Found: C, 76.05; H, 9.13; N, 6.17.

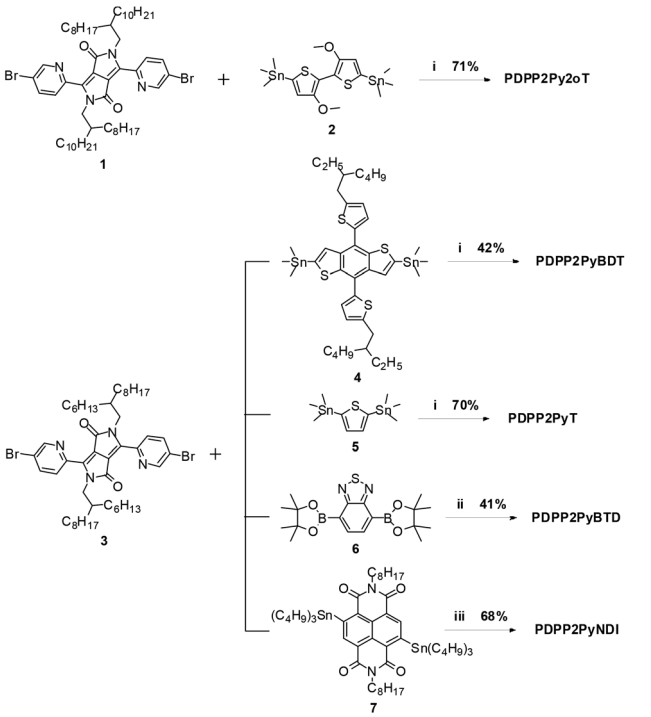

Scheme 1 Synthesis route of pyridine-bridged DPP polymers. (i) Stille polymerization by using $Pd_2(dba)_3/PPh_3$ in toluene/DMF (10 : 1, v/v) at 115 °C. (ii) Suzuki polymerization by using $Pd(PPh_3)_4/K_2CO_3$ (aq)/Aliquat 336 in toluene at 80 °C. (iii) Stille polymerization by using $Pd_2(dba)_3/PPh_3$/CuI in toluene/DMF (10 : 1, v/v) at 115 °C.

Results and discussion

Synthesis

The route for pyridine-bridged DPP polymers is shown in Scheme 1. **PDPP2Py2oT** was prepared by Stille polymerization with a bis(bromopyridinyl)-DPP monomer and a bisstannyl-bismethyloxy-bithiophene (2oT) monomer. Octyldodecyl (OD) side chains were applied to provide enough solubility for the polymer. A catalyst system based on $Pd_2(dba)_3$ as a source of palladium with PPh_3 as a ligand combined with the reaction solvent of toluene/DMF was used to achieve an optimized molecular weight. **PDPP2PyBDT** with benzodithiophene (BDT) and **PDPP2PyT** with thiophene (T) were also made *via* Stille polymerization with similar conditions to **PDPP2Py2oT**. For **PDPP2PyNDI** with electron withdrawing naphthadiimide (NDI), CuI was added into Stille polymerization to achieve high molecular weight.[43] We observed that the polymerization would not progress if CuI is absent. **PDPP2PyBTD** was polymerized by Suzuki polycondensation with $Pd(PPh_3)_4$ as a catalyst at 80 °C. The molecular weight of DPP polymers was determined by gel permeation chromatography (GPC) using *o*-dichlorobenzene (*o*-DCB) as an eluent. The GPC column was held at 140 °C and the polymer concentration was 0.1 mg ml^{-1} to reduce the aggregation of polymers. These polymers show a weight-average molecular weight (M_w) of 15.1–75.4 kg mol^{-1} but a high polydispersity index (PDI) of 2.39–6.63 (Table 1), so the number molecular weight (M_n) is modest (6.1–24.5 kg mol^{-1}). As shown in Fig. S1 (ESI†), low M_n and high PDI were quite different from thienyl-bridged DPP polymers.[44] This is probably due to the low reaction activity of dibromo-pyridine-bridged DPP monomers.

Optical and electrochemical properties

The DPP polymers show red-shifted absorption spectra in thin films (Fig. 2a) compared to those in chloroform solution (Table 1 and Fig. S2, ESI†), indicating aggregation. **PDPP2Py2oT** with strong donating 2oT units showed near-infrared absorption spectra with the absorption onset at 880 nm and an optical band gap (E_g) of 1.41 eV. Other pyridine-bridged DPP polymers show a similar wide band gap with an E_g of 1.75–1.85 eV. It is desired to mention that **PDPP2PyBTD** and **PDPP2PyNDI** with electron withdrawing BTD and NDI units show large band gaps of 1.76 eV and 1.85 eV. In comparison, their thienyl-bridged DPP polymers **PDPP2TBT** and PNDI-DPP have low band gaps of 1.19 eV[45] and 1.15 eV.[46] This huge difference indicates the great influence of pyridine as a bridge on their physical properties.

Table 1 Molecular weight, optical and electro-chemical properties of the pyridine-bridged DPP polymers

Polymer	M_n[a] (kg mol^{-1})	M_w[a] (kg mol^{-1})	PDI	$CHCl_3$ solution λ_{peak} (nm)	λ_{onset} (nm)	E_g^{sol} (eV)	Film λ_{peak} (nm)	λ_{onset} (nm)	E_g^{film} (eV)	LUMO[b] (eV)	HOMO[c] (eV)
PDPP2Py2oT	9.9	65.9	6.63	757	841	1.47	760	880	1.41	−3.80	−5.21
PDPP2PyBDT	24.1	75.4	3.13	665	690	1.80	665	708	1.75	−3.84	−5.59
PDPP2PyT	24.5	67.3	2.75	648	686	1.81	665	706	1.76	−3.89	−5.65
PDPP2PyBTD	6.1	15.1	2.49	585	663	1.87	628	704	1.76	−4.01	−5.77
PDPP2PyNDI	15.2	36.4	2.39	592	667	1.86	592	670	1.85	−4.22	−6.07

[a] Determined with GPC at 140 °C using *o*-DCB as the eluent. [b] Determined using a work function value of −5.23 eV for Fc/Fc^+. [c] Determined as $E_{LUMO} - E_g^{film}$.

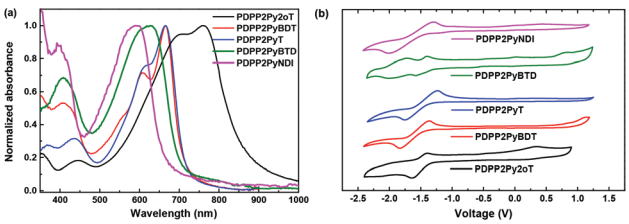

Fig. 2 (a) Optical absorption spectra of the polymers in solid state films and (b) cyclic voltammograms of the polymers in *o*-DCB. Potential *vs.* Fc/Fc^+.

The energy levels of DPP polymers were determined using cyclic voltammetry in *o*-DCB solutions (Fig. 2b and Table 1). When the electron donating ability decreased or the electron withdrawing ability increased, DPP polymers show increased HOMO and LUMO levels. **PDPP2Py2oT** has LUMO and HOMO levels of −3.80 eV and −5.21 eV. The low HOMO level will help hole injection in OFETs but also reduce V_{oc} in PSCs. **PDPP2PyBDT** and **PDPP2PyT** with BDT and T as donors show a similar LUMO level but a high HOMO level that is beneficial for high V_{oc} in PSCs. **PDPP2PyBTD** with electron withdrawing BTD units provides a LUMO level of −4.01 eV and a HOMO level of −5.77 eV. Further increase of LUMO and HOMO levels is realized by using NDI as a building block, in which **PDPP2PyNDI** shows a LUMO level of −4.22 eV and HOMO level of −6.07 eV. The LUMO and HOMO levels of **PDPP2PyNDI** are similar to fullerene derivatives, indicating its potential application as a non-fullerene electron acceptor for polymer–polymer solar cells. The great variation of energy levels induced by copolymerized aromatic units would influence their electronic properties in OFETs and PSCs.

Density functional theory (DFT) calculations at the B3LYP/6-31G level were performed for extended oligomers based on these DPP polymers. In the DFT calculations methyl units were used to replace long alkyl chains in order to reduce the calculation time. Deep HOMO and LUMO levels were achieved from a 2oT-based oligomer to a NDI-based oligomer (Fig. 3), which has a similar trend to the measured energy levels of DPP polymers. For **PDPP2Py2oT**, **PDPP2PyBDT** and **PDPP2PyT** with electron donating units, HOMO and LUMO orbitals are delocalized over the conjugated backbone. However, the HOMO levels of **PDPP2PyBTD** and **PDPP2PyNDI** are mainly

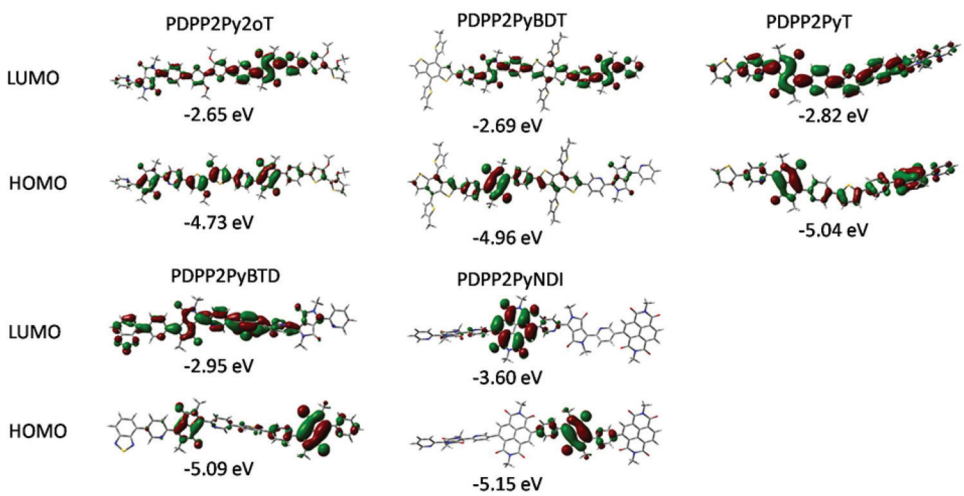

Fig. 3 DFT frontier molecular orbitals for the segments of pyridine-bridged DPP polymers.

delocalized over the DPP core and the LUMO levels are mainly delocalized over the BTD or NDI units. The dihedral angle between aromatic units and neighboring pyridine units is around 20° for **PDPP2Py2oT**, **PDPP2PyBDT** and **PDPP2PyT**. The dihedral angle was greatly increased to 38.20° for **PDPP2PyBTD** and 59.33° for **PDPP2PyNDI** (Fig. S3, ESI†).

Molecular stacking of DPP polymers was analyzed by X-ray diffraction (XRD) of the polymer thin films (Fig. 4 and S4, ESI†). All the pure polymer films drop casted from chloroform solutions displayed diffraction peaks (Fig. S4, ESI†) and the intensity of these peaks are increased after thermal annealing of thin films at 150 °C (Fig. 4). The polymers show strong (100) diffraction peaks at 2θ = 4.25° (**PDPP2Py2oT**), 4.31° (**PDPP2PyBDT**), 4.48° (**PDPP2PyBTD**) and 4.61° (**PDPP2PyNDI**). **PDPP2PyT** showed weak diffraction peaks at 2θ = 4.71°. The lamellar *d*-spacings are 1.87–2.08 nm (Fig. 4). **PDPP2PyBTD** and **PDPP2PyNDI** showed large dihedral angles (38.20° and 59.33°) on the conjugated backbone (Fig. S3, ESI†), but they still showed good crystallinity with *d*-spacings of 1.97 nm and 1.92 nm. **PDPP2PyBDT** also showed a weak and broad peak (010) at an angle of 24.21°, corresponding to the π–π stacking distance of 0.37 nm. For the other polymers, the (010) peak is too weak to be observed. GIWAXS was also applied to investigate the crystal behaviour of the polymers in thin films (Fig. S5, ESI†), showing that most of the polymers perform the diffraction in the small angle region (0.3–0.4 Å) in the in-plane and out-of-plane direction that corresponds to the stacking of alkyl side chains.

Charge carrier mobility

Charge carrier mobility of the DPP polymers was determined in a bottom gate–bottom contact FET configuration. A highly n-doped Si wafer with a SiO_2 layer which contained strip gold electrodes was passivated with octadecyltrichlorosilane (OTS) self-assembled monolayers. DPP polymers dissolved in chloroform or *o*-DCB were spin-coated on the substrates and moved into the glovebox with N_2. After annealing at the corresponding temperature, the devices were measured at room temperature. Representative transfer curves are shown in Fig. 5. The mobility (μ) in the saturated region and the threshold voltage (V_T) were calculated using the following equation:

$$I_{DS} = (W/2L)C_i\mu(V_G - V_T)^2$$

where W and L are the channel width and length, respectively, C_i is the unit dimensional dielectric capacitance of the gate insulator, μ is the field-effect mobility, and V_T is the threshold voltage.

All devices exhibit very high on/off ratios ($I_{on/off}$: 10^5–10^7). V_T is around −20 to −30 V for hole mobilities and 20–60 V for electron mobilities. **PDPP2Py2oT** only exhibits a hole mobility (μ_h) of 2.95 × 10^{-2} cm^2 V^{-1} s^{-1} (Table 2). OFETs based on **PDPP2PyBDT** and **PDPP2PyT** with weakly donating building blocks show typical ambipolar transfer characteristics (Fig. 5b and c). **PDPP2PyBDT** exhibited a higher μ_h of 2.60 × 10^{-2} cm^2 V^{-1} s^{-1} compared to its electron mobility (μ_e) of 2.67 × 10^{-3} cm^2 V^{-1} s^{-1}. However, **PDPP2PyT** showed higher μ_e of 1.34 × 10^{-2} cm^2 V^{-1} s^{-1} than the μ_h of 1.65 × 10^{-3} cm^2 V^{-1} s^{-1}. The trend of increased electron mobility and reduced hole mobility

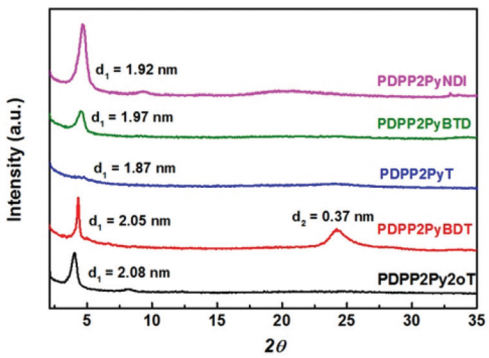

Fig. 4 X-ray diffraction patterns of the DPP polymers in thin films annealing at 150 °C for 10 min.

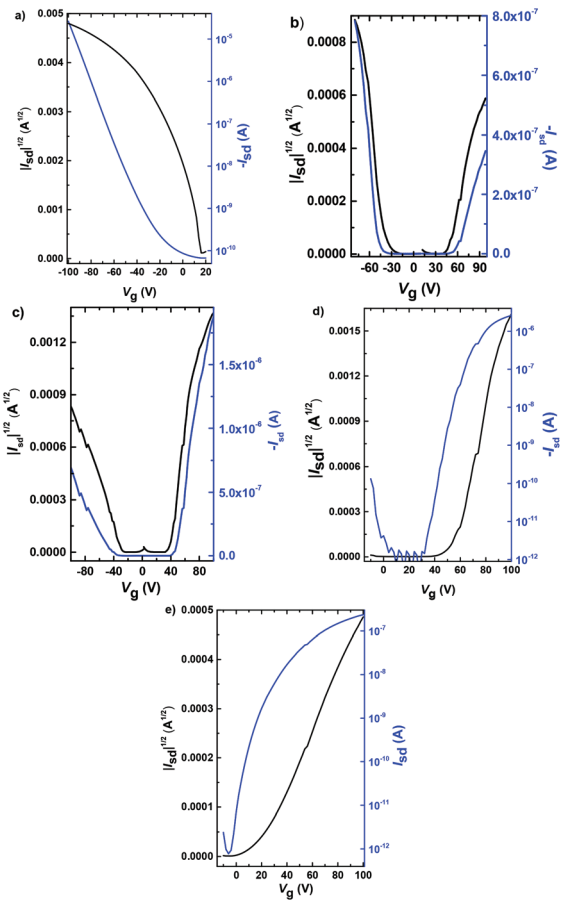

Fig. 5 Transfer characteristics of bottom-contact OFETs for the DPP polymers. (a) **PDPP2Py2oT**, (b) **PDPP2PyBDT**, (c) **PDPP2PyT**, (d) **PDPP2PyBTD** and (e) **PDPP2PyNDI**. *W*/*L* = 1400/50 μm, except for **PDPP2PyBTD** devices with *W*/*L* = 1400/10 μm.

Table 2 Field effect hole and electron mobility of the DPP polymers

Polymer	Annealing temperature[a] (°C)	μ_h ($cm^2\ V^{-1}\ s^{-1}$)	μ_e ($cm^2\ V^{-1}\ s^{-1}$)
PDPP2Py2oT	100	2.95×10^{-2}	—
PDPP2PyBDT	160	2.60×10^{-2}	2.67×10^{-3}
PDPP2PyT	100	1.65×10^{-3}	1.34×10^{-2}
PDPP2PyBTD	100	—	4.62×10^{-3}
PDPP2PyNDI	200	—	1.24×10^{-3}

[a] Annealing in a glovebox filled with N_2 under the temperature for 10 min.

Table 3 Solar cell parameters of optimized solar cells of the DPP polymers with [70]PCBM

Polymer[a]	Thickness (nm)	J_{sc} (mA cm^{-2})	V_{oc} (V)	FF	PCE (%)
PDPP2Py2oT	90	5.0	0.53	0.54	1.4
PDPP2PyBDT	100	4.7	0.86	0.55	2.2
PDPP2PyT	85	4.8	0.79	0.64	2.4

[a] The ratio of DPP-polymer to [70]PCBM is 1 : 2. The optimized spin coating solvent for the active layer is $CHCl_3$ with 5% DIO as an additive.

was probably due to increased LUMO and HOMO levels of DPP polymers. A deep LUMO level would help electron injection from the gold electrodes but a deep HOMO level is not beneficial for hole injection. Further enhancement of LUMO and HOMO levels for **PDPP2PyBTD** and **PDPP2PyNDI** provides the polymers only electron mobilities of around 10^{-3} $cm^2\ V^{-1}\ s^{-1}$. OFETs clearly showed that modification of polymer structures by introducing building blocks with different electron-donating or withdrawing abilities can effectively tune the energy level and hole or electron mobilities.

Photovoltaic properties

Pyridine-bridged DPP polymers as an electron donor blended with [70]PCBM as an electron acceptor were further applied to photovoltaic devices, sandwiched between the transparent ITO/PEDOT:PSS front and the reflecting Ca/Al back electrodes. The photoactive layers composed of DPP polymers and [70]PCBM were carefully optimized with respect to the ratio of the donor to the acceptor, the solvent with an additive and the layer thickness. **PDPP2PyBTD** and **PDPP2PyNDI** based cells have no photovoltaic effect due to their deep LUMO levels, which induced a low driving force for charge separation from the donor to the acceptor.

The *J–V* characteristics of **PDPP2Py2oT**, **PDPP2PyBDT** and **PDPP2PyT** based cells are presented in Fig. 6 and the photovoltaic parameters are shown in Table 3. In general, photoactive layers based on DPP-polymer:[70]PCBM for optimized cells were spin coated from a chloroform solution with 5 vol% 1,8-diiodooctane (DIO) as an additive and the ratio of the donor to the acceptor was 1 : 2. When using 1-CN or *o*-DCB as an additive, the solar cells provided lower PCEs (Table S1†). **PDPP2Py2oT** with the high-lying HOMO level showed a low V_{oc} of 0.53 V, and **PDPP2PyBDT** and **PDPP2PyT** showed a high V_{oc} of 0.86 V and 0.79 V due to their deep HOMO levels. All these cells gave a modest short circuit current density (J_{sc}) of 4.7–5.0 mA cm^{-2}, and a fill factor of 0.54–0.64. Therefore, the PCE based on DPP-polymer:[70]PCBM cells is 1.4% (**PDPP2Py2oT**), 2.2% (**PDPP2PyBDT**) and 2.4% (**PDPP2PyT**), which is much less than that for thienyl-bridged DPP polymers. The low PCE is mainly attributed to their low J_{sc} that also can be seen from their external quantum efficiency (EQE) (Fig. 6b). **PDPP2Py2oT**:[70]PCBM cells showed a low EQE (<0.1) contributed by the absorption of the polymer. **PDPP2PyBDT** and **PDPP2PyT** based cells also gave EQE lower than 0.35 in their absorption region. We also synthesized OD-**PDPP2PyT** with longer OD side chains so as to achieve high M_n = 39.9 kg mol^{-1} and PDI = 3.76 compared to the polymer with HD units (Scheme S1†), but the devices based on OD-**PDPP2PyT** provide a very poor PCE of 0.43% (Table S2†). The results confirm the previous observation that DPP polymers with longer side chains yield low efficiency solar cells.[47]

Low photon-conversion into electron efficiency based on these pyridine-bridged DPP polymers is desired to be discussed. It has been reported that in thienyl-bridged DPP polymer based photovoltaic cells, energy loss ($E_{Loss} = E_g - eV_{oc}$) between band gaps of the donor polymer to V_{oc} has a great influence on the EQE of devices.[20] In these pyridine-bridged DPP polymer solar cells, E_{Loss} was calculated to be 0.88 eV (**PDPP2Py2oT**), 0.89 eV (**PDPP2PyBDT**) and 0.97 eV (**PDPP2PyT**) that should be enough for exciton separation into free carriers. The poor EQE and PCE in these cells may originate from the poor phase separation between the polymer and [70]PCBM as shown in Fig. 7. In the AFM height image of photoactive layers, a large domain can be found in these polymer:[70]PCBM systems, indicating that the exciton has difficulty in diffusion into the interface of the donor and the acceptor. In addition, it should also be noted that the relatively low molecular weight of these pyridine-bridged DPP polymers indicates a possible defect on the conjugated backbone, such as the homo-coupling segment, which is detrimental to the photovoltaic device's performance.[48] A further study of the optimization of polymerization conditions to achieve high molecular

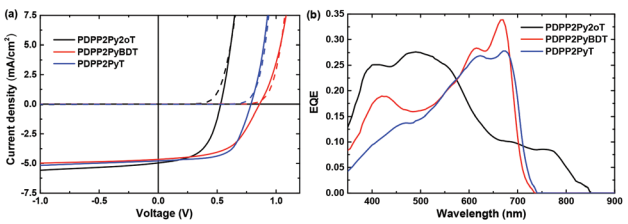

Fig. 6 (a) *J–V* characteristics in the dark (dashed lines) and under white light illumination (solid lines) of optimized solar cells of the polymers with [70]PCBM. (b) EQE of the same devices.

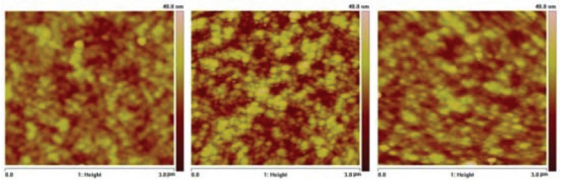

Fig. 7 AFM height image of the optimized DPP-polymer:[70]PCBM (1 : 2) spin-coated from chloroform containing 5 vol% DIO. (a) **PDPP2Py2oT**, (b) **PDPP2PyBDT** and (c) **PDPP2PyT**. Root mean square (RMS) roughness is 3.3 nm, 5.02 nm and 3.81 nm from **PDPP2Py2oT** to **PDPP2PyT**.

weight pyridine-bridged DPP polymers will be necessary to improve the PCE of photovoltaic cells.

Conclusions

A series of conjugated polymers with DPP as the core and pyridine as the bridge were designed and synthesized, where alternating building blocks from the electron donor to the electron acceptor were introduced. A strong electron donating unit, such as bimethoxy-dithiophene, was incorporated into DPP polymers with a low band gap of 1.41 eV. DPP polymers containing weak donors or electron acceptors as building blocks show wide band gaps of around 1.8 eV. The HOMO and LUMO levels of DPP polymers were influenced by incorporating building blocks, following the trends from strong donors to weak donors and electron acceptors. Therefore, the polarity of charge transport in OFETs can be varied from p-type for **PDPP2Py2oT** with strong donors to ambipolar behaviour for **PDPP2PyBDT** and **PDPP2PyT** alternating with weak donors and n-type for DPP polymers with electron withdrawing units. Further investigation of photovoltaic devices based on these polymers showed a modest PCE of 1.4–2.4% due to their low external quantum efficiency. The results show that the energy level and charge transport properties of conjugated polymers, from hole-only to ambipolar and electron-only transport, can be effectively tuned *via* copolymerized building blocks. Further investigation on improving the molecular weight is also needed for pyridine-bridged DPP polymers toward high performance photovoltaic devices.

Acknowledgements

We thank Ralf Bovee and Prof. René A. J. Janssen at Eindhoven University of Technology (Tue, Netherlands) for GPC analysis and Dr Jianqi Zhang at the National Center for Nanoscience and Technology (Beijing, China) for GIWAXS measurement. This work was supported by the Recruitment Program of Global Youth Experts of China. The work was further supported by the Ministry of Science and Technology of China (2014CB643600 and 2013CB933500) and the Strategic Priority Research Program (grant no. XDB12030300) of the Chinese Academy of Sciences.

Notes and references

1 C. B. Nielsen, M. Turbiez and I. McCulloch, *Adv. Mater.*, 2013, **25**, 1859–1880.
2 X. Guo, A. Facchetti and T. J. Marks, *Chem. Rev.*, 2014, **114**, 8943–9021.
3 M. M. Wienk, M. Turbiez, J. Gilot and R. A. J. Janssen, *Adv. Mater.*, 2008, **20**, 2556–2560.
4 A. C. Rochat, L. Cassar and A. Iqbal, *Euro Pat*, 94911, 1983.
5 I. Kang, T. K. An, J.-a. Hong, H.-J. Yun, R. Kim, D. S. Chung, C. E. Park, Y.-H. Kim and S.-K. Kwon, *Adv. Mater.*, 2013, **25**, 524–528.
6 H. J. Chen, Y. L. Guo, G. Yu, Y. Zhao, J. Zhang, D. Gao, H. T. Liu and Y. Q. Liu, *Adv. Mater.*, 2012, **24**, 4618–4622.
7 I. Kang, H.-J. Yun, D. S. Chung, S.-K. Kwon and Y.-H. Kim, *J. Am. Chem. Soc.*, 2013, **135**, 14896–14899.
8 J. Y. Back, H. Yu, I. Song, I. Kang, H. Ahn, T. J. Shin, S.-K. Kwon, J. H. Oh and Y.-H. Kim, *Chem. Mater.*, 2015, **27**, 1732–1739.
9 J. H. Park, E. H. Jung, J. W. Jung and W. H. Jo, *Adv. Mater.*, 2013, **25**, 2583–2588.
10 K. H. Hendriks, G. H. L. Heintges, V. S. Gevaerts, M. M. Wienk and R. A. J. Janssen, *Angew. Chem., Int. Ed.*, 2013, **52**, 8341–8344.
11 R. S. Ashraf, I. Meager, M. Nikolka, M. Kirkus, M. Planells, B. C. Schroeder, S. Holliday, M. Hurhangee, C. B. Nielsen, H. Sirringhaus and I. McCulloch, *J. Am. Chem. Soc.*, 2014, **137**, 1314–1321.
12 H. Bronstein, Z. Chen, R. S. Ashraf, W. Zhang, J. Du, J. R. Durrant, P. Shakya Tuladhar, K. Song, S. E. Watkins, Y. Geerts, M. M. Wienk, R. A. J. Janssen, T. Anthopoulos, H. Sirringhaus, M. Heeney and I. McCulloch, *J. Am. Chem. Soc.*, 2011, **133**, 3272–3275.
13 I. Meager, R. S. Ashraf, S. Mollinger, B. C. Schroeder, H. Bronstein, D. Beatrup, M. S. Vezie, T. Kirchartz, A. Salleo, J. Nelson and I. McCulloch, *J. Am. Chem. Soc.*, 2013, **135**, 11537–11540.
14 K. H. Hendriks, W. Li, M. M. Wienk and R. A. J. Janssen, *J. Am. Chem. Soc.*, 2014, **136**, 12130–12136.
15 L. Dou, W.-H. Chang, J. Gao, C.-C. Chen, J. You and Y. Yang, *Adv. Mater.*, 2013, **25**, 825–831.
16 C. H. Woo, P. M. Beaujuge, T. W. Holcombe, O. P. Lee and J. M. J. Fréchet, *J. Am. Chem. Soc.*, 2010, **132**, 15547–15549.
17 A. T. Yiu, P. M. Beaujuge, O. P. Lee, C. H. Woo, M. F. Toney and J. M. J. Frechet, *J. Am. Chem. Soc.*, 2012, **134**, 2180–2185.
18 L. T. Dou, J. Gao, E. Richard, J. B. You, C. C. Chen, K. C. Cha, Y. J. He, G. Li and Y. Yang, *J. Am. Chem. Soc.*, 2012, **134**, 10071–10079.
19 B. Carsten, J. M. Szarko, L. Lu, H. J. Son, F. He, Y. Y. Botros, L. X. Chen and L. Yu, *Macromolecules*, 2012, **45**, 6390–6395.
20 W. Li, K. H. Hendriks, A. Furlan, M. M. Wienk and R. A. J. Janssen, *J. Am. Chem. Soc.*, 2015, **137**, 2231–2234.
21 L. T. Dou, J. B. You, J. Yang, C. C. Chen, Y. J. He, S. Murase, T. Moriarty, K. Emery, G. Li and Y. Yang, *Nat. Photonics*, 2012, **6**, 180–185.

22 J. You, L. Dou, K. Yoshimura, T. Kato, K. Ohya, T. Moriarty, K. Emery, C.-C. Chen, J. Gao, G. Li and Y. Yang, *Nat. Commun.*, 2013, **4**, 1446.

23 W. Li, A. Furlan, K. H. Hendriks, M. M. Wienk and R. A. J. Janssen, *J. Am. Chem. Soc.*, 2013, **135**, 5529–5532.

24 O. Adebanjo, P. P. Maharjan, P. Adhikary, M. Wang, S. Yang and Q. Qiao, *Energy Environ. Sci.*, 2013, **6**, 3150–3170.

25 C. Kanimozhi, P. Balraju, G. D. Sharma and S. Patil, *J. Phys. Chem. B*, 2010, **114**, 3095–3103.

26 W. Li, A. Furlan, W. S. C. Roelofs, K. H. Hendriks, G. W. P. van Pruissen, M. M. Wienk and R. A. J. Janssen, *Chem. Commun.*, 2014, **50**, 679–681.

27 J. W. Jung, F. Liu, T. P. Russell and W. H. Jo, *Chem. Commun.*, 2013, **49**, 8495–8497.

28 Y. J. Cheng, S. H. Yang and C. S. Hsu, *Chem. Rev.*, 2009, **109**, 5868–5923.

29 Y. P. Zou, D. Gendron, R. Badrou-Aich, A. Najari, Y. Tao and M. Leclerc, *Macromolecules*, 2009, **42**, 2891–2894.

30 J. Jo, D. Gendron, A. Najari, J. S. Moon, S. Cho, M. Leclerc and A. J. Heeger, *Appl. Phys. Lett.*, 2010, **97**, 203303–203303.

31 E. Zhou, S. Yamakawa, K. Tajima, C. Yang and K. Hashimoto, *Chem. Mater.*, 2009, **21**, 4055–4061.

32 L. Huo, J. Hou, H.-Y. Chen, S. Zhang, Y. Jiang, T. L. Chen and Y. Yang, *Macromolecules*, 2009, **42**, 6564–6571.

33 A. P. Zoombelt, S. G. J. Mathijssen, M. G. R. Turbiez, M. M. Wienk and R. A. J. Janssen, *J. Mater. Chem.*, 2010, **20**, 2240–2246.

34 G. Lange and B. Tieke, *Macromol. Chem. Phys.*, 1999, **200**, 106–112.

35 T. Beyerlein and B. Tieke, *Macromol. Rapid Commun.*, 2000, **21**, 182–189.

36 T. Beyerlein, B. Tieke, S. Forero-Lenger and W. Brütting, *Synth. Met.*, 2002, **130**, 115–119.

37 M.-F. Falzon, A. P. Zoombelt, M. M. Wienk and R. A. J. Janssen, *Phys. Chem. Chem. Phys.*, 2011, **13**, 8931–8939.

38 W. Li, T. Lee, S. J. Oh and C. R. Kagan, *ACS Appl. Mater. Interfaces*, 2011, **3**, 3874–3883.

39 L. Chen, D. Deng, Y. Nan, M. Shi, P. K. L. Chan and H. Chen, *J. Phys. Chem. C*, 2011, **115**, 11282–11292.

40 C. Kim, J. Liu, J. Lin, A. B. Tamayo, B. Walker, G. Wu and T.-Q. Nguyen, *Chem. Mater.*, 2012, **24**, 1699–1709.

41 B. Sun, W. Hong, Z. Yan, H. Aziz and Y. Li, *Adv. Mater.*, 2014, **26**, 2636–2642.

42 T. H. Marks and A. Facchetti, *US Pat*, 8859714, 2014.

43 L. E. Polander, A. S. Romanov, S. Barlow, D. K. Hwang, B. Kippelen, T. V. Timofeeva and S. R. Marder, *Org. Lett.*, 2012, **14**, 918–921.

44 W. Li, K. H. Hendriks, A. Furlan, W. S. C. Roelofs, M. M. Wienk and R. A. J. Janssen, *J. Am. Chem. Soc.*, 2013, **135**, 18942–18948.

45 W. Li, K. H. Hendriks, A. Furlan, A. Zhang, M. M. Wienk and R. A. J. Janssen, *Chem. Commun.*, 2015, **51**, 4290–4293.

46 P. Wang, H. Li, C. Gu, H. Dong, Z. Xu and H. Fu, *RSC Adv.*, 2015, **5**, 19520–19527.

47 W. Li, K. H. Hendriks, A. Furlan, W. S. C. Roelofs, S. C. J. Meskers, M. M. Wienk and R. A. J. Janssen, *Adv. Mater.*, 2014, **26**, 1565–1570.

48 K. H. Hendriks, W. Li, G. H. L. Heintges, G. W. P. van Pruissen, M. M. Wienk and R. A. J. Janssen, *J. Am. Chem. Soc.*, 2014, **136**, 11128–11133.